Sensitivity analysis of a model of CO2 exchange in tundra ecosystems by the adjoint method

C. Waelbroeck, J.-F. Louis

JOURNAL OF GEOPHYSICAL RESEARCH, VOL. 100, NO. D2, PAGES 2801–2816, FEBRUARY 20, 1995

Sensitivity analysis of a model of CO_2 exchange in tundra ecosystems by the adjoint method

C. Waelbroeck
Laboratoire de Modélisation du Climat et de l'Environnement, Gif-sur-Yvette, France

J.-F. Louis
Atmospheric and Environmental Research, Incorporated, Cambridge, Massachusetts

Abstract. A model of net primary production (NPP), decomposition, and nitrogen cycling in tundra ecosystems has been developed. The adjoint technique is used to study the sensitivity of the computed annual net CO_2 flux to perturbations in initial conditions, climatic inputs, and model's main parameters describing current seasonal CO_2 exchange in wet sedge tundra at Barrow, Alaska. The results show that net CO_2 flux is most sensitive to parameters characterizing litter chemical composition and more sensitive to decomposition parameters than to NPP parameters. This underlines the fact that in nutrient-limited ecosystems, decomposition drives net CO_2 exchange by controlling mineralization of main nutrients. The results also indicate that the short-term (1 year) response of wet sedge tundra to CO_2-induced warming is a significant increase in CO_2 emission, creating a positive feedback to atmospheric CO_2 accumulation. However, a cloudiness increase during the same year can severely alter this response and lead to either a slight decrease or a strong increase in emitted CO_2, depending on its exact timing. These results demonstrate that the adjoint method is well suited to study systems encountering regime changes, as a single run of the adjoint model provides sensitivities of the net CO_2 flux to perturbations in all parameters and variables at any time of the year. Moreover, it is shown that large errors due to the presence of thresholds can be avoided by first delimiting the range of applicability of the adjoint results.

1. Introduction

Global climate models predict an increase in global mean temperature of 1.3 to 5.2°C resulting from a doubling of atmospheric CO_2 [*Schlesinger and Mitchell*, 1987; *Gates et al.*, 1992]. However, the biophysical processes responsible for CO_2 exchanges at the surface are governed by climatic conditions, so that feedback mechanisms to climate change might dramatically alter the present source and sink pattern and the consequences of the greenhouse effect.

In the climate change context, tundra ecosystems could play a particularly important role because of the very large amount of organic carbon buried in their soils, e.g., 50 to 60 kg C m^{-2} on the Alaskan North Slope [*Jenkinson et al.*, 1991] and because of the expected larger increase in temperature at high latitudes than at low latitudes [*Mitchell et al.*, 1990; *Gates et al.*, 1992]. Therefore our purpose is to investigate the relationship between carbon fluxes and climate in tundra ecosystems and, more specifically, to estimate the response of these ecosystems to climate change. We present here a model calculating CO_2 fluxes and soil carbon accumulation or loss in the tundra as a function of a few climatic variables and analyze its sensitivity to changes in climatic conditions, initial carbon compartment size, and soil and vegetation parameters. Because of the large number of parameters and variables influencing the net CO_2 flux exchanged between the ecosystem and the atmosphere, we use the adjoint method to perform the sensitivity study. The advantages and drawbacks of the method are also examined.

Paper number 94JD02831.
0148-0227/95/94JD-02831$05.00

2. The Model

2.1. Introduction

The net CO_2 flux exchanged between terrestrial biosphere and atmosphere is the balance among three distinct processes: photosynthesis, plant respiration, and soil organic matter decomposition (also called soil respiration). Net primary production (NPP) is the part of the total amount of organic matter created by photosynthesis that remains after some of this material is used in the respiration of plants. In other words, NPP is the amount of organic matter accumulated in plant tissues per unit time and corresponds to an uptake of atmospheric CO_2 by the ecosystem. In contrast, decomposition results in a flux directed toward the atmosphere. This flux is released by oxidation of dead plant material by bacterial and fungal decomposers which utilize the energy, carbon, and other nutrients released by the process.

NPP and decomposition depend on climate in a very complex way. While the surface climatic conditions directly influence plant photosynthesis and respiration, decomposition is driven by the soil temperature and moisture regime which is itself related to the presence of permafrost [*Bonan*, 1989; *Waelbroeck*, 1993]. Also, the total amount of CO_2 released by decomposition depends on the litter input rate

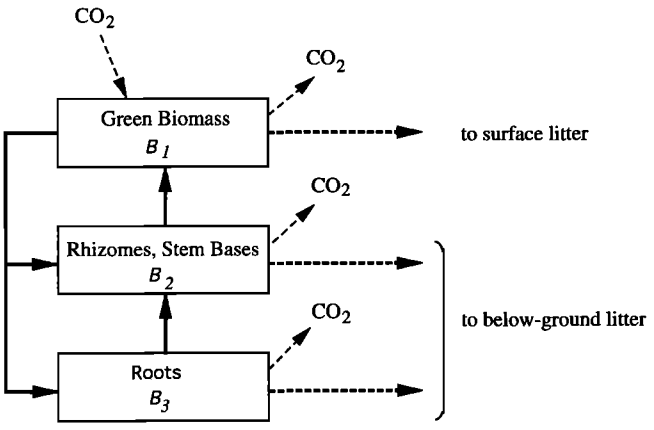

Figure 1. Diagram of plant C fluxes. Solid arrows represent live biomass flows; thick dashed arrows represent dead biomass flows and thin dashed arrows represent CO_2 fluxes.

which, in turn, depends on surface climatic conditions and soil thermal regime through plant growth and death rates. Similarly, photosynthesis not only depends on surface climatic conditions (e.g., air temperature, solar irradiance) but also on atmospheric CO_2 concentration and on the amount of nutrients available for plant growth. In the particular case of tundra ecosystems, measurements of photosynthetic rates at elevated CO_2 levels showed that within 3 to 4 weeks, plants maintained at ambient and elevated CO_2 levels had similar photosynthetic rates [*Tissue and Oechel*, 1987; *Grulke et al.*, 1990; *Oechel and Billings*, 1992]. These results are in agreement with other observations which show that growth in the field in tundra ecosystems is more limited by nutrient supply than by carbohydrates [*Billings et al.*, 1984; *Shaver and Kummerow*, 1992]. Therefore because decomposition plays a central role in the cycling of essential nutrients (e.g., nitrogen and phosphorus), soil temperature and moisture conditions also indirectly influence NPP.

The model described in the present section does not incorporate all the details of the current knowledge of photosynthesis, plant respiration, plant carbon allocation, and decomposition processes. Instead, the omission of details in the present model is deliberate and represents our attempt to formulate a model of general applicability, which provides estimates on a regional scale.

Another important feature of the model is that it is designed as a tool to study the response of tundra ecosystems to changes in climatic conditions and to analyze and quantify all the feedbacks induced by these changes. Consequently, the model is based on the explicit parameterization of the biophysical processes involved in carbon exchanges and not on regression laws.

Finally, the present model includes nutrient cycling and the effect of nutrient limitation on the ecosystem production. Since most of nutrient replenishment is accomplished by mineralization of organic nitrogen and phosphorus through the action of decomposer microorganisms, climate change, by affecting the decomposition rate, will induce changes in the mineralization rate and therefore in the amount of nutrients available.

There exist some models of carbon fluxes in the tundra which are based on the biophysical description of NPP and decomposition but lack a description of nutrient cycling [*Bunnell and Scoullar*, 1975; *Miller et al.*, 1984]. More recently, *Rastetter et al.* [1991] developed and applied to tundra a general biogeochemical model of the C and N cycles in terrestrial ecosystems. However, these models do not explicitly calculate the soil temperature and moisture regime. In the case of tundra ecosystems, any prediction based on the assumption that soil temperature variations simply parallel air temperature variations is erroneous because the soil thermal regime strongly depends on the soil moisture content which, in turn, depends, among other things, on the depth to permafrost which greatly differs under warmer or colder climatic conditions. Consequently, in order to account for the nonlinearities and feedbacks present in the soil-plant-climate system, it is necessary to explicitly parameterize all the physical processes which link climatic variables to carbon fluxes. Therefore our approach has been to develop the present decomposition and NPP model in conjunction with a physical model of the soil temperature and moisture regimes in the presence of permafrost [*Waelbroeck*, 1993].

2.2. Net Primary Production (NPP) Submodel

The model considers three live biomass pools: aboveground green biomass, B_1, rhizomes and stem bases, B_2, and roots, B_3 (Figure 1). The model describes the average vegetation present at a given site, without distinction between species. It does not therefore simulate species changes and is limited to the time period before shift in vegetation boundaries modifies important vegetation parameters (i.e., 50–100 years). A time step of 1 day has been chosen to correctly describe the seasonal cycle.

The existence of a very complete data set for the coastal tundra at Barrow, Alaska, allowed us to accurately validate the model. The numerical values given in the present paper correspond to Barrow's vegetation and soil.

Photosynthesis. Photosynthesis is controlled by climatic conditions, on one hand, and by nutrient supply on the other hand. Potential photosynthesis is computed as a function of climatic conditions:

$$PS_{\text{pot}} = PS_{\max} B_1 \text{ solf tmpf} \quad (1)$$

where PS_{pot} is the potential photosynthetic rate (g C m^{-2} d^{-1}); $PS_{\max}$ is the maximum relative photosynthetic rate (g C g C^{-1} d^{-1}); B_1 is the current amount of green biomass (g C m^{-2}); solf is a solar factor (0–1); and tmpf is a temperature factor (0–1).

Based on the generally linear patterns of daily leaf photosynthetic rates versus daily radiation and the very low compensation points found by *Tieszen* [1978] and by *Limbach et al.* [1982] for tundra plants, the light dependence of leaf photosynthesis is assumed to vary linearly from 0 to 1 for increasing levels of solar radiation. The solar factor for the whole vegetation cover is obtained by correcting the leaf solar factor for the effect of shading:

$$\text{solf} = \frac{S}{S_{\max}} [0.5 + 0.5e^{-0.7\,\text{LAI}}] \quad (2)$$

where S is the incoming solar radiation (W m^{-2}), $S_{\max}$ is the annual maximum solar radiation level (W m^{-2}), and LAI is the leaf area index: LAI = LSA B_1 with LSA the leaf specific area (m^2 g C^{-1}).

The temperature factor is taken from *Bunnell and Scoullar* [1975]. Photosynthesis is assumed to take place for air temperatures comprised between −2°C and 30°C, with an optimal temperature of 15°C:

$$\text{tmpf} = tf(T_a;\ -2,\ 15,\ 30) \tag{3}$$

with $tf(T;\ T_{\min},\ T_{\text{opt}},\ T_{\max})$ defined in Figure 2.

As stated in the introduction, decomposition, photosynthesis, and nutrient uptake are represented in a simplified way, designed to capture the relationships between these processes and climatic variables. In this context we only considered one limiting nutrient with respect to plant primary production, namely, mineral nitrogen.

The critical level of nutrient availability under which there is production limitation is defined as the ratio of the potential photosynthesis rate by the average plant C/N ratio (Figure 3). In case of nutrient limitation the actual photosynthesis rate on a given day is taken proportional to the sum of the maximum amount of nutrient available on that day in the plants and in the soil:

$$PS = \min\ \{PS_{\text{pot}},\ cn(F_l + F_{\min})\} \tag{4}$$

where cn is the average plant C to N ratio, $F_l = N_l\ \text{d}^{-1}$ with N_l, the current amount of plant labile N (g N m^{-2}), and $F_{\min} = N_{\min}\ \text{d}^{-1}$ with $N_{\min}$, the current amount of soil mineral N (g N m^{-2}). In this formulation the nitrogen necessary to synthesize new material is first taken in the plant labile N pool and then in the soil.

The plant labile N pool is assumed to be replenished by the N flow made of N which was bonded to the C lost in plant respiration so that N_l is given by

$$\frac{dN_l}{dt} = \frac{\text{total plant respiration}}{cn} - \min\left\{F_l,\ \frac{PS_{\text{pot}}}{cn}\right\} \tag{5}$$

Soil mineral nutrients availability in tundra ecosystems is governed by soil decomposition. This assumption is based on measurements of respiration and mineralization rates in six Arctic soils by *Nadelhoffer et al.* [1991]. We will describe in the following section how $N_{\min}$ is determined as part of the soil N cycle.

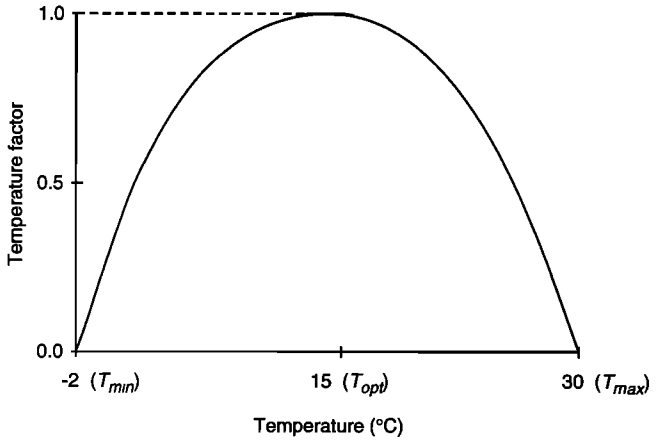

Figure 2. Temperature factor for photosynthesis and growth.

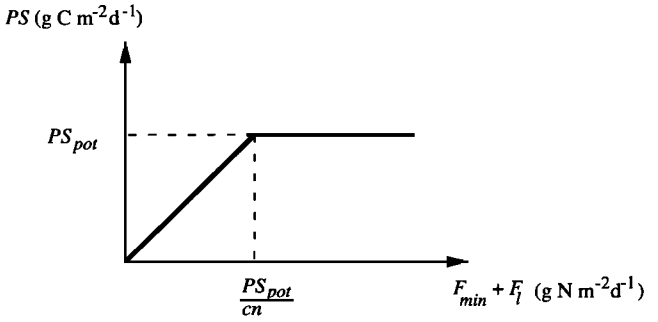

Figure 3. Effect of N limitation on photosynthesis.

Respiration. The total respiration rate is the sum of maintenance and growth respiration rates for each plant part. Maintenance respiration is computed as a function of the compartment size and the average air or soil temperature, according to the formula

$$\text{RESP}_i = r_i\ B_i\ 2^{\left(\frac{T-10}{10}\right)} \tag{6}$$

where r_i is the relative maintenance respiration rate of biomass pool (i) at 10°C (g C g C^{-1} d^{-1}). T is either the daily mean air temperature T_a, the surface temperature T_s, or the soil temperature at half depth of the organic layer, T_{soil}, expressed in °C; respectively, for leaf, rhizome, or root respiration.

Growth respiration of each biomass compartment is assumed to be a constant fraction, α_{gr}, of the amount of growth of that compartment; $\alpha_{gr} \approx 0.3$ [*Bunnell and Scoullar*, 1975; *Running and Coughlan*, 1988].

Growth. The scheme adopted for the allocation of newly photosynthesized material (photosynthate) within the plant is based on *Bunnell and Scoullar* [1975]. However, in their model, growth rates are calculated as a fixed fraction of the available photosynthate, whereas the present model accounts for the dependence of growth rates on temperature and nutrient availability.

First, potential growth rates of aboveground biomass and roots are calculated as the product of a maximum daily growth rate, a temperature function, and an allocation factor so that more photosynthate is allocated to roots than to leaves in case of nutrient limitation:

$$\begin{aligned} GR_{\text{pot1}} &= G_{\max 1}\ B_1\ \text{lftf lfall} \\ \text{GR}_{\text{pot3}} &= G_{\max 3}\ B_3\ \text{rttf rtall} \end{aligned} \tag{7}$$

where $G_{\max i}$ is the maximum relative growth rate of biomass pool (i) (g C g C^{-1} d^{-1}): lftf = $tf(T_a,\ 1.5,\ 15,\ 28.5)$; rttf = $tf(T_{\text{soil}},\ -2,\ 15,\ 30)$; lfall = 0.9, in presence of nutrient limitation; = 1, otherwise; and rtall = 1.1, in presence of nutrient limitation; = 1, otherwise. (Optimal and threshold temperature are from *Miller et al.* [1984].)

Then, actual root and green biomass growth rates are taken as the minimum between potential growth rate and available photosynthate in the following order: The amount of photosynthate available for green growth is assumed to be equal to the total amount of photosynthate minus total maintenance respiration costs; the amount of photosynthate available for root growth is then equal to what is left after

Table 1. Equations Used to Calculate Plant C Translocation and Death Rates

Equation	Condition
$TR_{21} = \frac{TR_{max21}}{5}$ (Julian-bgs)B_2	if bgs < Julian ≤ bgs + 5
$TR_{21} = TR_{max21}\left(1 - \frac{\text{(Julian-bgs} - 5)}{10}\right)B_2$	if bgs + 5 < Julian ≤ bgs + 15
$TR_{21} = 0$	otherwise
$TR_{23} = TR_{max23}\frac{0.21(B_2 - 0.85B_{max2})B_2}{0.15B_{max2}}$	if $0.85\,B_{max2} < B_2 \leq B_{max2}$
$TR_{23} = TR_{max23}\,B_2$	if $B_{max2} < B_2$
$TR_{23} = 0$	if $B_2 \leq 0.85B_{max2}$
$DTH_1 = \frac{D_{max1}}{0.09}(0.04B_1 - (GR_1 + TR_{21}))$	if $-0.05B_1 < GR_1 + TR_{21} < 0.04B_1$
$DTH_1 = D_{max1}\,B_1$	if $GR_1 + TR_{21} \leq -0.05B_1$
$DTH_2 = D_{max2}\,B_2$	if $0 < T_s$
$DTH_3 = \frac{D_{max3}}{0.007}(RESP_3 - (GR_3 + TR_{23}))$	if $-0.007B_3 < GR_3 + TR_{23} - RESP_3 < 0$
$DTH_3 = D_{max3}\,B_3$	if $GR_3 + TR_{23} - RESP_3 < -0.007B_3$

bgs, Julian day corresponding to the beginning of the growing season.
$D_{max\,i}$, maximum relative death rate of biomass compartment (i), g C g C^{-1} d^{-1}.
DTH_i, death rate of biomass compartment (i), g C m^{-2} d^{-1}.
TR_{ij}, translocation flux from biomass pool (i) to biomass pool (j), g C g C^{-1} d^{-1}.
$TR_{max\,ij}$, maximum relative translocation rate, g C m^{-2} d^{-1}.
T_s, average daily surface temperature, °C.

green growth, i.e., $PS - \sum_{i=1}^{3} RESP_i - GR_1$. If photosynthate is still available after maintenance respiration, green growth and root growth have been met, the remainder is allocated to rhizomes and stem bases. Finally, if there is not enough photosynthate to meet maintenance respiration (i.e., $PS < \sum_{i=1}^{3} RESP_i$), maintenance costs are shared by the three biomass compartments according to their relative size.

Therefore since growth rates are limited by the amount of photosynthate available, the simulated decrease in PS in case of nutrient limitation results in a decrease in growth rates.

C translocation and death rates. The parameterization of C allocation and death rates is based on *Bunnell and Scoullar* [1975]. The equations used are given in Table 1. In addition to allocation of new material through photosynthesis, as we just described, the model simulates translocations up from rhizomes and stem bases to green biomass in the spring, as well as translocations from rhizomes to roots when the rhizomes biomass exceeds a given value, B_{max2}.

Aboveground green biomass and roots are assumed to die when more carbon is respired than acquired through direct allocation of newly formed photosynthate or through translocation of photosynthate from other plant parts. Green biomass death rate is assumed to increase with decreasing growth rates and root death rate is assumed to increase as the net flux of carbon into roots decreases from 0 to a given negative value. Finally, rhizomes are assumed to die at a constant rate as soon as soil surface temperature rises above 0°C.

A fraction, α_{12} of green biomass death rate and α_{32} of root death rate, represents the amount of biomass that is withdrawn to rhizomes when green biomass and roots die. Consequently, the daily surface litter input is given by $(1 - \alpha_{12})DTH_1$ and daily belowground litter input, by $(1 - \alpha_{32})DTH_3 + DTH_2$.

The budget equations of carbon in the three biomass compartments and plant labile N form a set of four ordinary differential equations which are coupled to the equations of the decomposition submodel through litter input (Figure 1) and nutrient limitation. Its solution gives us plant biomass and C fluxes on every day of the year. One can then estimate the daily NPP, i.e., the daily C flux from the atmosphere toward the plants:

$$\text{NPP} = PS - \text{total plant respiration}$$

$$= PS - \sum_{i=1}^{3} RESP_i - \alpha_{gr} \sum_{i=1}^{3} GR_i \qquad (8)$$

2.3. Decomposition Submodel

The structure of the decomposition component of our model is based on the Century model [*Parton et al.*, 1987], which describes the climatic and textural controls of soil organic matter (SOM) in Great Plains grasslands. We adopted Century's structure because it not only computes the CO_2 flux toward the atmosphere but also organic carbon and nitrogen flows in the soil, resulting from dead organic matter decomposition so that the amount of available nutrient can be estimated easily. However, whereas in Century, aboveground and belowground primary production are estimated as a function of annual precipitation by regression equations (based on grasslands data sets), the computation of primary production in our model is based on the full parameterization of photosynthesis, plant respiration, growth, and death rates (section 2.2).

Soil C cycle. Like Century, our model contains several SOM pools with different characteristic turnover times (Figure 4). Litter input on a given day is the amount of biomass which dies on that day. Dead green biomass forms surface litter, whereas dead roots and rhizomes form soil litter. Plant residue is partitioned between woody and herbaceous litter according to its lignin to N ratio, *ln* (Appendix A). Since lignin is much more resistant to decomposition than cellulose or hemicellulose, the turnover of woody litter is much longer than that of herbaceous litter. Litter is broken down by the decomposer microorganisms, giving rise to CO_2, but also to organic matter under a different physical or chemical form with more biological resistance to decomposition. These "secondary" decomposition products are represented by two SOM pools, namely, the active SOM and slow SOM pools. A permafrost pool has been added to the set of pools usually present in decomposition models in order to simulate the response of soil decomposition to changes in permafrost depth. Its decay rate is assumed to be zero since SOM in that pool is isolated from O_2 and nutrient sources so that biological activity cannot be sustained. Note that the six first SOM compartments do not correspond to separate physical entities: indeed, organic soil at a given depth in the active layer (i.e., above permafrost) contains a mixture of organic matter at various stages of decomposition. However, one can assume that organic soil located below the maximum rooting depth contains older and more resistant C on the average than organic soil above that level. This is why we assume that when the permafrost table rises or lowers, the permafrost SOM pool exchanges organic matter only with the slow SOM pool (Figure 4).

The amount of SOM which is decomposed per unit time in pool (i) is given by

$$\frac{dC_i(t)}{dt} = -k_i(t)C_i(t) \tag{9}$$

where C_i is the amount of C contained in pool (i) (g C m^{-2}); k_i is the decay rate of pool (i) (day^{-1}) (in other words, k_i^{-1} is the turnover time of pool (i)). The total carbon flux out of pool (i) given by (9) is partitioned between CO_2 emission and SOM flows according to *Parton et al.* [1987] (see Figure 4).

Decay rates depend on soil temperature and moisture in the following manner:

$$k_i(t) = K_i \text{ tfn mfn} \tag{10}$$

where K_i is the characteristic decay constant of pool (i); tfn and mfn are, respectively, the effect of soil temperature and soil moisture. The influence of substrate chemical composition (i.e., lignin content) and of soil texture on decay constants is modeled as in Century (Appendix A).

Based on measurements by *Flanagan and Veum* [1974], the temperature dependence of decay rates is represented by

$$\text{tfn} = a\ 4^{\left(\frac{T_{soil}-10}{10}\right)} \qquad \text{if } -7.5°C < T_{soil} \le 15°C$$

$$\text{tfn} = -a\frac{(T_{soil}-2.5)(T_{soil}-45)}{187.5} \qquad \text{if } 15°C < T_{soil} \le 45°C \tag{11}$$

$$\text{tfn} = 0 \qquad \text{otherwise}$$

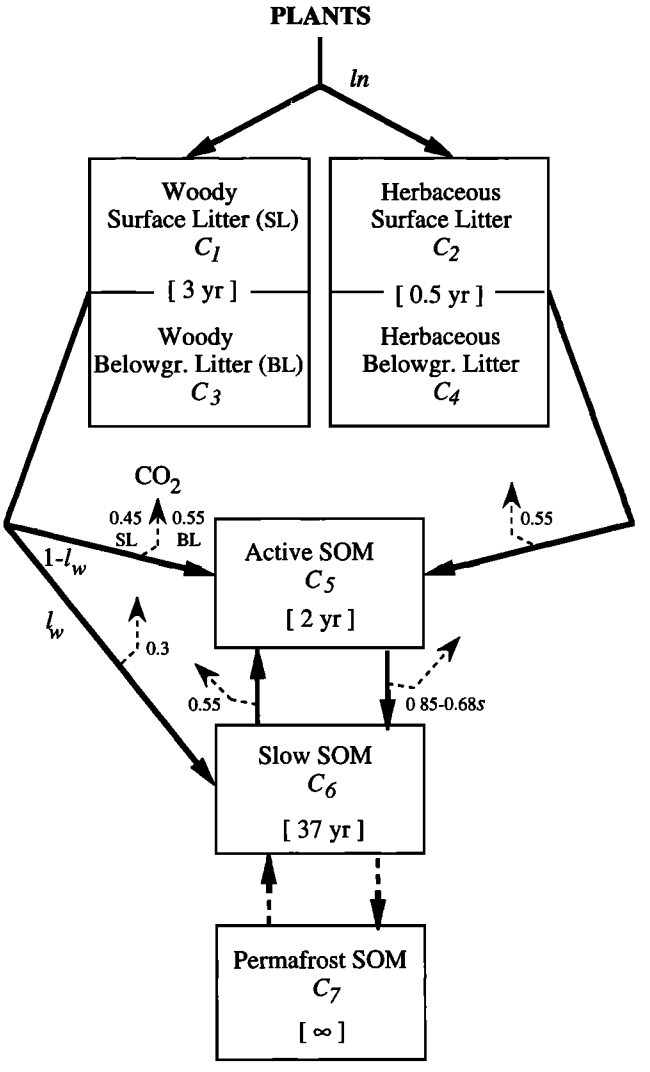

Figure 4. Diagram of the soil organic matter (SOM) decomposition submodel. Solid arrows represent SOM flows and thin arrows, CO_2 emission. Thick dashed arrows represent SOM exchanges resulting from variations in permafrost depth. Turnover times at optimal temperature and moisture are indicated between brackets; *ln*, plant lignin to N ratio; l_w, woody litter lignin fraction; s, soil silt plus clay fraction.

where a = 0.15 is the average ratio between measured respiration rates at 10°C and at optimal moisture content reported by *Flanagan and Veum* [1974] and those deduced from *Parton et al.*'s [1987] representation.

Soil respiration increases with increasing moisture until an optimum moisture content is reached and then decreases for further increases in soil moisture, due to reduced O_2 availability. Based on *Rastetter et al.* [1991], we adopted the following formulation of mfn:

$$\text{mfn} = b\left(\frac{m^c - m_{opt}^c}{m_{opt}^c - 1000^c}\right)^2 \tag{12}$$

where m is the organic soil moisture content (% dry weight), m_{opt} = 200% dry weight is the optimal moisture content, b and c are parameters, respectively, equal to 0.2 and −0.5.

Whereas the amount of organic C in the six SOM pools

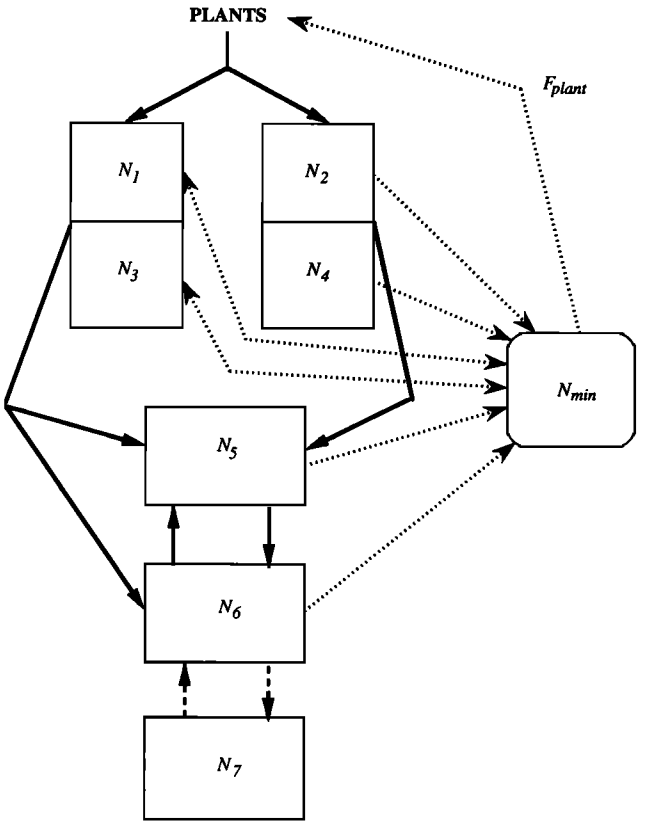

Figure 5. Scheme of the soil N cycle. Thick arrows represent organic N flows and thin arrows, mineral N flows.

located in the active layer and the resulting total CO_2 flux due to decomposition are computed daily, the amount of carbon imprisoned in permafrost, C_7, is calculated once a year according to the annual increment in permafrost depth. To convert annual increments in permafrost depth into SOM, we defined an average SOM volumetric content, ρ_7 (g C m^{-3}), based on current data:

$$\rho_7 = \frac{\text{total active layer SOM}}{\text{active layer depth}} \tag{13}$$

Consequently, in areas where organic matter is locked in the permafrost, a lowering of the permafrost table induces a SOM flux from the permafrost pool to the slow SOM pool, making it available to decomposers.

Soil N cycle. As in Century, the basic assumption here is that most N is bonded to organic C (Figure 5). Soil N flows are assumed to be equal to the product of the corresponding C flows and the N to C ratio of the SOM pool that receives N. The C to N ratios of the different SOM pools are given in Table 2. Organic N is converted into mineral nitrogen pool and conversely as a result of biological activity. On one hand, the nitrogen that was bonded to the organic C lost as CO_2 through respiration is converted from organic to inorganic form. This is represented by a mineralization flux from the SOM pools to the mineral N pool, equal to the product of the C flow lost as CO_2 and the N to C ratio of the SOM pool it leaves. On the other hand, when the amount of N is too low to sustain microbial activity in a given organic pool, microbial demand for mineral nutrient induces immobilization, i.e., conversion of mineral N to organic N. The "net" mineralization flux from a given organic pool (i) to the mineral N pool is computed as the N flow necessary to balance the N budget in that particular organic pool:

$$\text{MIN}_i = -\frac{dN_i(t)}{dt} + \sum_{j \neq i}^{6} \left(\frac{F_{ji}}{cn_i} - \frac{F_{ij}}{cn_j} \right) \qquad i = 1, \cdots, 6 \tag{14}$$

with

$$\frac{dN_i(t)}{dt} = \frac{1}{cn_i} \frac{dC_i(t)}{dt}$$

where F_{ji} is the organic carbon flow from pool (j) to (i) (g C m^{-2} d^{-1}); and cn_i is the C/N ratio of pool (i).

Finally, the daily budget of soil mineral N is obtained by the difference between the total net mineralization and the plant N uptake flux deduced from (4)

$$\frac{dN_{\text{min}}}{dt} = \sum_{i}^{6} \text{MIN}_i - \min \left\{ F_{\text{min}}, \max \left\{ 0, \frac{PS_{\text{pot}}}{cn} - F_l \right\} \right\} \tag{15}$$

In summary, the budget equations of the active layer organic C and of soil mineral N form a set of seven ordinary differential equations coupled to the four equations describing the plants C and N budget. This set of 11 differential equations is discretized in time and integrated from initial conditions with a time step of one day by using a Runge-Kutta numerical scheme of the fourth order. In contrast, permafrost SOM content is computed with a time step of one year (equation (13)).

Since measurements of initial SOM compartment sizes are not available in practice, we assumed that organic matter is distributed among the active layer SOM pools according to fractions deduced from the steady state solution of the budget equations of active layer organic C, corresponding to a constant input flow of new litter and constant decay rates (Appendix B). Note that only two measurements are needed per site: the total amount of organic C per unit area in the active layer and the amount of organic C in permafrost. The partition of soil organic matter among the various active layer pools obtained by this method is close to the initial compartment sizes given by *Bunnell and Scoullar* [1975].

The model has been validated in different sites of wet sedge tundra. The parameter values used in the present

Table 2. C to N Ratios of Soil Organic Matter Pools

SOM Pool	C/N Ratio
Pool 1, surface woody litter	150[a]
Pool 2, surface herbaceous litter	...[b]
Pool 3, soil woody litter	150[a]
Pool 4, soil herbaceous litter	...
Pool 5, active SOM	max {14 − N_{min}4, 6}[a]
Pool 6, slow SOM	max {18 − N_{min}3, 12}[a]

SOM, soil organic matter.
[a]*Parton et al.* [1987].
[b]Herbaceous litter pools are assumed to contain the remainder of the incoming plant residue N after the C/N ratio of woody litter is met.

sedge tundra. The parameter values used in the present study are those used to successfully reproduce measured CO_2 fluxes at Prudhoe Bay in 1990 and 1991 and at Barrow in 1992 (W. C. Oechel et al., personal communication, 1993). They are included in Table 4. The results of this validation will be described in details by C. Waelbroeck and W. C. Oechel (manuscript in preparation, 1995).

3. Adjoint Method for Sensitivity Analysis

In the following sections we study the sensitivity of the CO_2 flux with respect to the initial conditions, to the model parameters, independent of time, and the climatic inputs, which vary in time. We want to examine not only the effect of a constant change of these quantities but also how perturbations at specific times of the year may affect the net CO_2 flux. For example, the effect of a soil temperature increase at the beginning of the growing season may be quite different from the effect of the same perturbation later in the year.

The adjoint method is very well suited to this purpose. It provides an efficient way to compute the gradient of a complicated compound function of a set of arguments and hence to study the sensitivity of a model output to a large number of parameters and variables. In contrast to the classical method, which consists in perturbing each control variable (or parameter) and computing the corresponding variation in the model's output, thus requiring as many integrations of the model as there are control variables, the adjoint technique only requires one integration of the model itself and one integration of the adjoint model. Therefore the gain in computational time is enormous for problems with a large number of control variables and parameters.

Examples of applications where the computation of large dimension gradients are required are sensitivity analysis of one model result to many parameters [*Hall et al.*, 1982; *Errico and Vukićević*, 1992], optimization of model parameters with respect to one cost function [*Louis and Živković*, 1994], and variational data assimilation and inversion [*Le Dimet and Talagrand*, 1986; *Thépaut and Moll*, 1990]. A detailed description of the theory of the adjoint equation is given by *Talagrand and Courtier* [1987] and other publications (see an extensive bibliography in the work by *Courtier et al.* [1993]). In this section we briefly define the adjoint model and the notation used in the present study.

Let us represent the foregoing model as a nonlinear operator (or set of equations), R, acting on the initial state vector (or input), ξ_0, in a series of discrete steps:

$$\xi_N = R(\xi_0) = R_N R_{N-1} \cdots R_1(\xi_0) \tag{16}$$

The evolution of a small perturbation of the initial state is described by the tangent linear model (TLM):

$$\delta\xi_N = R' \delta\xi_0 = R'_N R'_{N-1} \cdots R'_1 \delta\xi_0 \tag{17}$$

where the operators R'_n are linear operators obtained by differentiating R_n. If R_n is nonlinear then R'_n depends on the state ξ_n.

For any scalar function of the output state vector, $J(\xi_N)$, it can be shown that its gradient with respect to the model input, $\nabla_{\xi_0} J$, obeys the equation

$$\nabla_{\xi_0} J = R'^* \nabla_{\xi_N} J = R'^*_1 R'^*_2 \cdots R'^*_N \nabla_{\xi_N} J \tag{18}$$

where R'^* is the adjoint model. This follows directly from a property of the inner product in a Hilbert space, which can be summarized as follows:

$$\delta J = \langle \nabla_{\xi_N} J,\ \delta\xi_N \rangle = \langle \nabla_{\xi_N} J,\ R' \delta\xi_0 \rangle = \langle R'^* \nabla_{\xi_N} J,\ \delta\xi_0 \rangle$$

$$= \langle \nabla_{\xi_0} J,\ \delta\xi_0 \rangle \tag{19}$$

To simplify the notation, we call ξ^* the adjoint variable $\nabla_\xi J$. Once R'^* has been developed, $\nabla_{\xi_0} J$ is given by ξ^*_0, the solution of (18). The initial condition for (18), ξ^*_N is easily computed since J is a simple function of ξ_N. In a discrete model such as ours, R'^*_n is simply the transpose of the matrix R'_n. This notation highlights the fact that the adjoint model is integrated backward: from step N to step 0. It represents the evolution of the sensitivity of J to the model state, as one steps farther and farther back through its history.

In the present case, J is defined as the annual net CO_2 flux: J = decomposition − NPP. R_n represents the operator corresponding to the model computation on Julian day $n(N = 365)$, and ξ_n is the state vector at the end of the nth day. In practice, the state vector ξ_n is extended to include all the parameters of the model and J itself [*Hoffman et al.*, 1992]:

$$\xi_n = \begin{pmatrix} \mathbf{X}_n \\ \boldsymbol{\alpha} \\ \mathbf{clim}_n \\ J_n \end{pmatrix} \tag{20}$$

where $\mathbf{X}_n$ is a column vector containing the values of the 11 state variables, $C_1, C_2, \cdots, C_6, B_1, \cdots, B_3, N_{min}$, and N_I at the end of the nth day; $\boldsymbol{\alpha}$ is a column vector of 36 elements containing the model's essential decomposition and NPP parameters: ln, l_w, PS_{max}, $\cdots$, which are constant throughout the run; $\mathbf{clim}_n$ is a column vector containing the values of the five climatic variables required to calculate NPP and soil decomposition on Julian day n (i.e., T_a, T_s, T_{soil}, m, and S); and J_n is the partial sum of the annual net CO_2 flux cumulated at the end of the nth day.

With these notations, $J = J_N$ and the input vector of the adjoint model, ξ^*_N, is a column vector of zeros with 1 as last element. The output of the adjoint model, $\xi^*_0 = \nabla_{\xi_0} J$, gives the sensitivity of the annual net CO_2 flux with respect to the initial conditions $\mathbf{X}_0$, model parameters $\boldsymbol{\alpha}$, and climatic variables $\mathbf{clim}_0$, all at once:

$$\nabla_{\xi_0} J = \begin{pmatrix} \nabla_{\mathbf{x}_0} J \\ \nabla_{\alpha_0} J \\ \nabla_{\mathbf{clim}_0} J \\ 1 \end{pmatrix} \tag{21}$$

This interpretation of the output of the adjoint code can be generalized to any time step n: ξ^*_n gives the sensitivity of J to a perturbation of the state variables, parameters, or climatic variables, applied on day n and maintained until day N.

4. Results

Control values of the parameters and current average climatic conditions at Barrow, Alaska, give an annual net

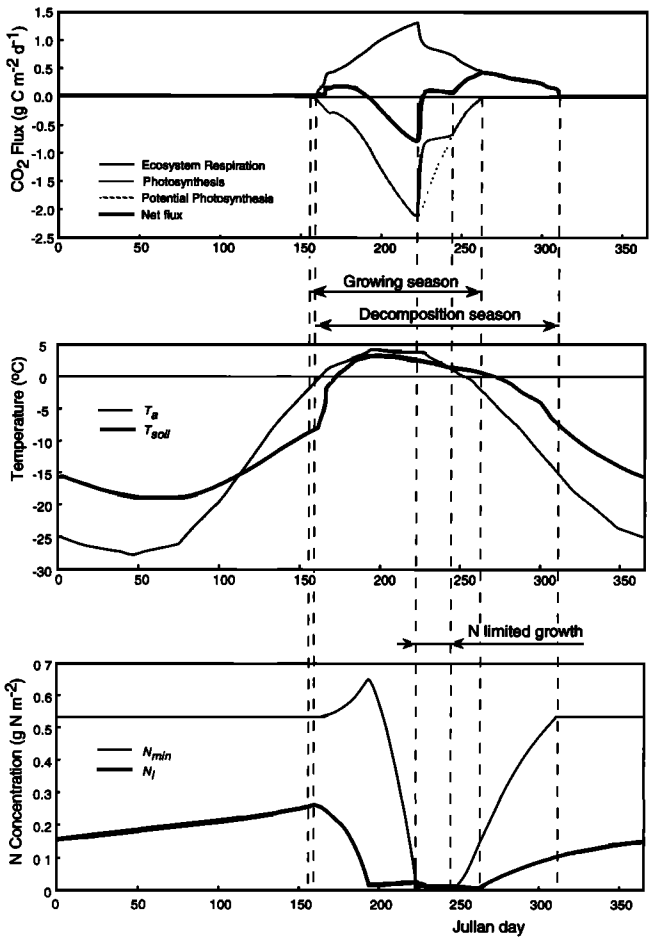

Figure 6. (top) Simulated total ecosystem respiration, photosynthesis, and net flux. (middle) Soil surface and air temperature used as inputs. (bottom) Simulated soil mineral N and plant labile N cycles.

flux, J, of approximately 17 g C m^{-2} yr^{-1}, i.e., a net source to the atmosphere. The seasonal cycle of the net CO_2 flux for the chosen standard conditions is plotted in Figure 6. CO_2 exchange is characterized by several distinct regimes. As explained in section 2, very low CO_2 emission, representing background maintenance respiration, occurs during the coldest period of the year. The system switches to another regime when surface or soil temperature crosses the −7.5°C threshold (middle panel of Figure 6), above which decomposition takes place (equation (11)). This "decomposition season" extends from Julian day 156 to 311. The growing season, during which photosynthesis takes place, corresponds to air temperature above −2°C (equation (3)) and extends from day 155 to 262. Another important change in CO_2 exchange regime occurs between day 221 and day 243. During that period, photosynthesis is controlled by the amount of mineral N available (Figure 6, bottom panel), whereas during the rest of the growing season, mineral N is not limiting and photosynthesis is determined by climatic conditions only (equation (4)).

It should be stressed that the dates and flux intensities given here were obtained with interpolated mean monthly climatic data. They are representative of the CO_2 average seasonal cycle at Barrow but would change somewhat if other climatic inputs were used. Table 3 lists the various CO_2 exchange regimes encountered along the year in our control simulation.

4.1. Sensitivity of the Annual Net CO_2 Flux to the Model Parameters

Table 4 gives the sensitivity of the annual net flux to a perturbation of the model parameters equal to 1% of their value and applied on Julian day 1. Following section 3, the values listed in Table 4 correspond thus to the subvector $\nabla_{\alpha_0} J$ of the adjoint output vector $\nabla_{\xi_0} J$ (equation (21)) multiplied by the perturbation $\delta\alpha = 0.01\alpha$.

The parameters are ranked by decreasing importance in terms of their impact on the annual net CO_2 flux. One sees that the parameters with the largest impact on the annual net flux are decomposition parameters. For instance, a 1% change in plant average lignin to N ratio, ln, produces a 7.6% change in net CO_2 flux. The large impact of decomposition parameters is easily explained by the fact that they affect not only soil respiration but also NPP, through their action on the mineralization of essential nutrients (and hence on actual photosynthesis). In this context, the plant lignin to N ratio plays an especially important role because it determines the amount of woody versus herbaceous litter (Appendix A), each being characterized by very different decomposition rates (i.e., woody litter is more resistant than herbaceous litter).

The output of the adjoint model consists in 365 vectors corresponding to 365 days of the year. Each vector contains the gradients of J with respect to perturbations applied to the variables and parameters on the corresponding Julian day and maintained until the end of the year. The difference $\xi^*_{n-1} - \xi^*_n$ is therefore the contribution of day n to the sensitivity, and the net yearly sensitivity of J to ξ is the sum of all those contributions. In other words, if we consider the evolution of one particular adjoint variable $\alpha^*(= \nabla_\alpha J)$, the slope of the α^* curve indicates the importance of a particular day for the net sensitivity, with the reverse sign because the adjoint is integrated backward in time.

As an example, the slope of $\nabla_{K_{max1}} J$ is zero before day 156

Table 3. CO_2 Exchange Regimes

Regime Description	Mathematical Definition	Dates
Decomposition season	T_s or $T_{soil} > -7.5$°C → decomp > 0	156–311
Growing season	$T_a > -2$°C → $PS > 0$	155–262
Plant N uptake from the soil	$\min\left\{F_{mm}, \max\left\{0, \frac{PS_{pot}}{cn} - F_l\right\}\right\} > 0$	192–257
N-limited growth	$PS < PS_{pot}$	221–243
Optimal green growth	$GR_1 = GR_{pot1}$	170–173; 241

Table 4. Sensitivity of the Annual Net CO_2 Flux to the Model Parameters

Parameter, α		Parameter Nominal Value	δ[Annual Net Flux], g C m^{-2} yr^{-1}, Induced by $\delta\alpha = 1\%\alpha$
Decomposition Parameters			
Plant lignin/N ratio	ln	40 g lignin g N^{-1}	−1.308
Woody litter lignin fraction	l_w	0.25	−0.513
Surface woody litter maximum decay	K_{max1}	10.9×10^{-3} d^{-1}	+0.490
Decay rates conversion factor (equation (11))	a	0.15	+0.360
Optimal soil moisture content	m_{opt}	200% dry weight	+0.250
Soil woody litter maximum decay	K_{max3}	13.4×10^{-3} d^{-1}	+0.162
Active SOM maximum decay	K_{max5}	20×10^{-3} d^{-1}	−0.155
Surface herbaceous litter maximum decay	K_{max2}	40×10^{-3} d^{-1}	−0.143
Moisture factor parameter (equation (12))	b	0.2	+0.139
Plant C/N ratio	cn	32 g C g N^{-1}	−0.133
Soil silt and clay fraction	s	0.73	+0.117
Active SOM maximum C/N ratio	cn_{max5}	14 g C g N^{-1}	−0.096
Moisture factor parameter (equation (12))	c	−0.5	+0.066
Active SOM fraction in organic layer	f	0.26	−0.040
Slow SOM maximum decay	K_{max6}	0.5×10^{-3} d^{-1}	+0.024
Soil herbaceous litter maximum decay	K_{max4}	50×10^{-3} d^{-1}	−0.019
Active SOM minimum C/N ratio	cn_{min5}	6 g C g N^{-1}	−0.014
Soil woody litter C/N ratio	cn_3	150 g C g N^{-1}	+0.014
Surface woody litter C/N ratio	cn_1	150 g C g N^{-1}	+0.012
Slow SOM maximum C/N ratio	cn_{max6}	18 g C g N^{-1}	−0.007
Slow SOM minimum C/N ratio	cn_{min6}	12 g C g N^{-1}	−0.003
Net Primary Production Parameters			
Root maintenance respiration at 10°C	r_3	0.002 g C g C^{-1} d^{-1}	+0.034
Leaf maximum death rate	D_{max1}	0.15 g C g C^{-1} d^{-1}	+0.018
Maximum relative photosynthetic rate	PS_{max}	0.16 g C g C^{-1} d^{-1}	−0.012
Rhizomes maintenance respiration at 10°C	r_2	0.002 g C g C^{-1} d^{-1}	+0.011
Leaf fraction translocated to rhizomes	α_{12}	0.25	+0.009
Leaf maintenance respiration at 10°C	r_1	0.008 g C g C^{-1} d^{-1}	+0.008
Maximum transpiration rate from rhizomes to leaves	TR_{max21}	0.03 g C g C^{-1} d^{-1}	+0.004
Root maximum death rate	D_{max3}	0.003 g C g C^{-1} d^{-1}	−0.003
Leaf specific area	LSA	0.03 m^{-2} g C^{-1}	+0.001
Rhizome maximum death rate	D_{max2}	0.001 g C g C^{-1} d^{-1}	−0.001
Growth respiration coefficient	α_{gr}	0.3	−0.001
Leaf maximum growth rate	G_{max1}	0.8 g C g C^{-1} d^{-1}	−0.001
Root fraction translocated to rhizomes	α_{32}	0.1	~+0.000
Maximum transpiration rate from rhizomes to roots	TR_{max23}	0.21 g C g C^{-1} d^{-1}	~−0.000
Root maximum growth rate	G_{max3}	1 g C g C^{-1} d^{-1}	0.000

and after day 304 (Figure 7), indicating that when the surface temperature is too low for decomposition, there is no sensitivity of the CO_2 flux to K_{max1}. The rest of the year the slope of the curve is always negative, corresponding to a positive sensitivity. This is explained by the fact that when decomposition of surface woody litter takes place, an increase in K_{max1} induces an increase in the decomposition rate of surface woody litter (equations (10) and (A1)) and hence in soil respiration and CO_2 net flux. This increase is large during the growing season because an increase in K_{max1} during that period induces a decrease in NPP and thus a further increase in J. Indeed, an increase in the decomposition rate of surface woody litter induces not only an increase in respiration but also an increase in organic matter transfers to the active SOM and slow SOM pools (Figure 4). As a result, the organic C content of the active and slow SOM pools increase, while that of surface woody litter decreases, with corresponding changes in organic N. Because the C/N ratio of woody litter is an order of magnitude larger than that of the active or slow SOM (Table 2), the net effect of these changes is to decrease the net mineralization rate (equation (14)). Therefore an increase in K_{max1} results in a decrease in the amount of soil mineral N and thus in a decrease in NPP. Note that this effect does not take place after day 243 because NPP is not limited by nutrient availability any longer after that date (Figure 6, bottom panel).

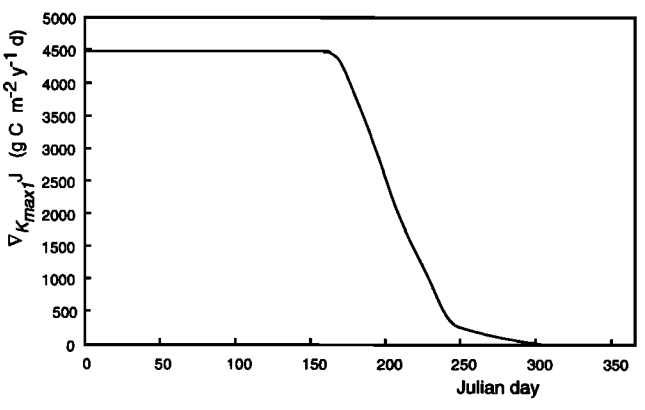

Figure 7. Sensitivity of the annual net CO_2 flux to the maximum decay rate of surface woody litter, K_{max1}.

Instead of monotonously increasing or decreasing during the year, an adjoint variable curve can have an extremum on

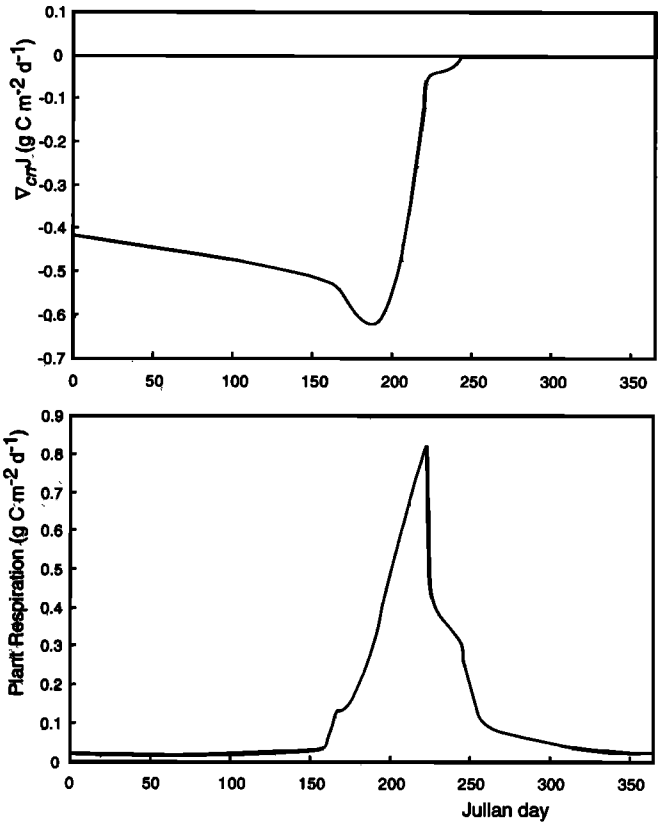

Figure 8. (top) Sensitivity of the annual net CO_2 flux to the average plant C to N ratio, cn. (bottom) Simulated total plant respiration.

a given day. The top panel of Figure 8 shows an example of such a behavior, for $\nabla_{cn}J$. Before day 192 the slope of the curve is negative, indicating that during that period a localized increase of cn has a positive impact on the yearly CO_2 flux. After day 192, however, the slope is positive, meaning that an increase of cn now has a negative impact on the CO_2 flux. Positive sensitivities to increases in cn applied at the beginning of the year illustrate the fact that an increase in cn induces a decrease in N_l (equation (5)) which results in a decrease in NPP and thus an increase in J. The steeper slope between ≈166 and 192 indicates that the increase in J due to an increase in cn is stronger after the beginning of the growing season because the total plant respiration flux increases sharply after that date (Figure 8, bottom panel).

From day 198 to 258 the plant has to take up soil mineral N to supply its photosynthate requirements (Figure 6, bottom panel) so that an increase in cn strongly lessens the effect of nutrient limitation by reducing the required daily soil mineral N uptake (equation (4)). This strong negative effect overcomes the previous positive effect after day 192.

Note that the slope at the beginning of the year is different from the one at the end of the year because during the winter a change in cn does not affect the yearly CO_2 flux directly but indirectly through a change in N_l. The effect on the CO_2 flux is therefore delayed until the beginning of the growing season, when a decrease in N_l has an impact on J. A change in cn in the fall would not affect J until the next year's growing season. Since our computation stops at the end of the first year, J is not sensitive to cn after day 262.

4.2. Sensitivity of the Annual Net CO_2 Flux to the Initial Conditions

Table 5 lists, in decreasing order of importance, the changes in J induced by a 1% change in the values of the state variables on day 1. One sees that changes in the initial conditions only weakly affect the annual net CO_2 flux. The change in J induced by a 1% change in B_1 is particularly small because on one hand, the sensitivity to $B_1(0)$ is weak, as it is to $B_2(0)$ and $B_3(0)$, and on the other hand, B_1 itself is quasi-nil in the winter. The sensitivity to the initial value of a variable that reduces to almost zero in the winter, like B_1, has little significance. It is only included here for completeness.

4.3. Sensitivity of the Annual Net CO_2 Flux to the Model's Climatic Inputs

Table 6 gives, in order of decreasing importance, the changes in J induced by an increase in daily climatic variables equal to 1% of the amplitude of their seasonal cycle, applied on every day of the year (starting on day 1), and Figures 9a–9e show the corresponding complete adjoint curves.

One sees that the surface and soil temperature, T_s and T_{soil}, have the largest impact on J (Figure 9). This translates the fact that an increase in T_s (or T_{soil}) induces an increase in both soil decomposition and rhizome (or root) respiration. Figure 9a also indicates that the increase in J due to an increase in T_s is reinforced during the beginning of the

Table 5. Sensitivity of the Annual Net CO_2 Flux to the Initial Conditions

Variable, X	Variable Initial Value, $X(0)$	δ[Annual Net Flux], g C m^{-2} yr^{-1} Induced by $\delta X = 1\% X(0)$
Surface woody litter, C_1	1530.389 g C m^{-2}	+0.295
Soil woody litter, C_3	718.204 g C m^{-2}	+0.098
Soil mineral N, N_{min}	0.533 g N m^{-2}	−0.094
Active SOM, C_5	842.863 g C m^{-2}	−0.093
Surface herbaceous litter, C_2	24.842 g C m^{-2}	−0.091
Plant labile, N_l	0.156 g N m^{-2}	−0.030
Roots, B_3	48.625 g C m^{-2}	+0.019
Slow SOM, C_6	15962.787 g C m^{-2}	+0.016
Soil herbaceous litter, C_4	4.409 g C m^{-2}	−0.011
Rhizomes, B_2	16.643 g C m^{-2}	+0.009
Green biomass, B_1	0.006 g C m^{-2}	~−0.000

Table 6. Sensitivity of the Annual Net CO_2 Flux to the Model Climatic Inputs

Climatic Variable	δclim = 1% Seasonal Cycle Amplitude	δ[Annual Net Flux], g C m^{-2} yr^{-1}
Soil surface temperature, T_s	0.29°C	+1.396
Air temperature, T_a	0.33°C	−0.463
Organic soil moisture, m	1.9% dry weight	−0.180
Soil temperature, T_{soil}	0.23°C	+0.097
Solar radiation, S	2.49 W m^{-2}	−0.065

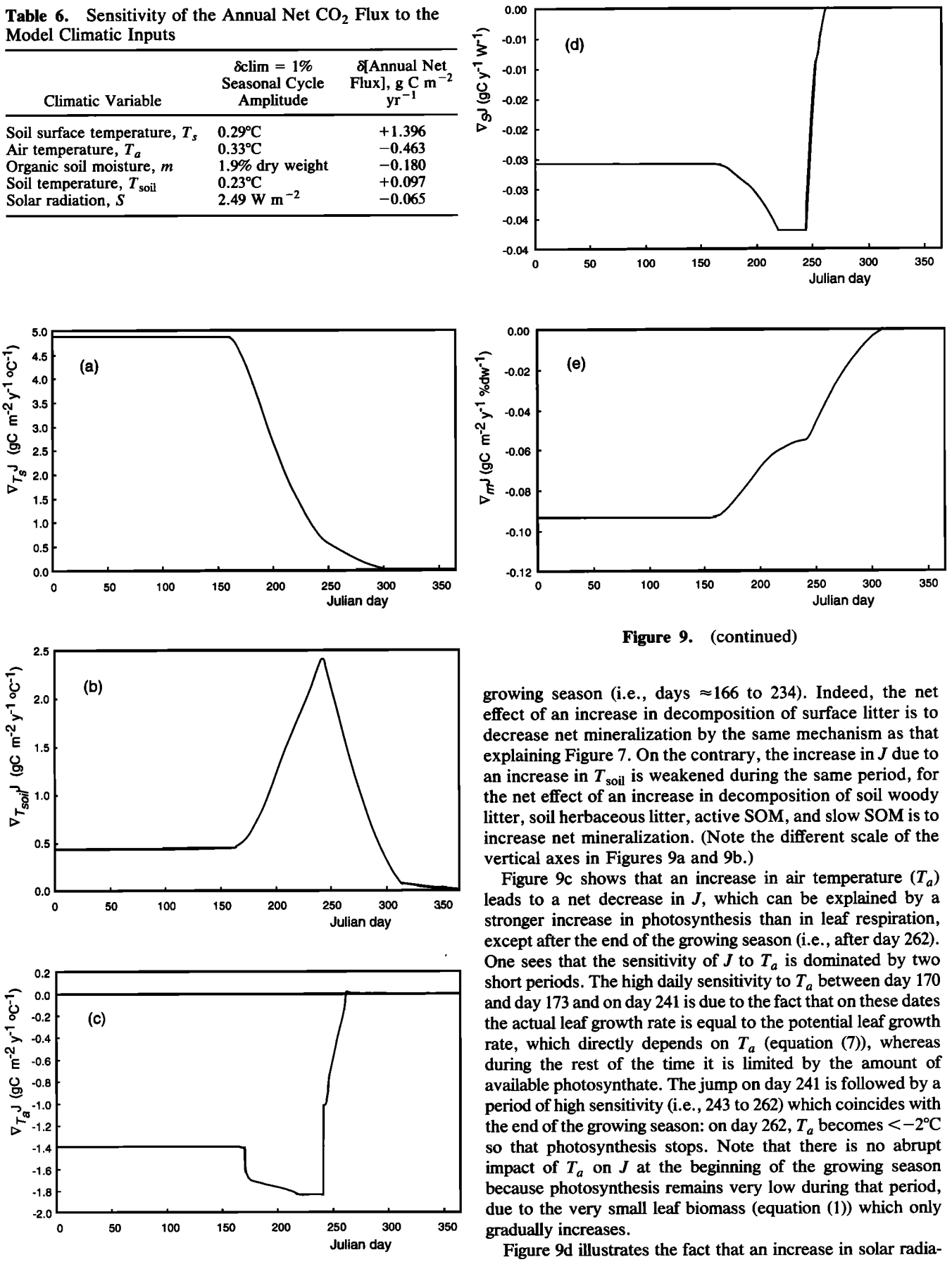

Figure 9. Sensitivity of the annual net CO_2 flux to climatic inputs: (a) $\nabla_{T_s}J$; (b) $\nabla_{T_{soil}}J$; (c) $\nabla_{T_a}J$; (d) $\nabla_S J$; (e) $\nabla_m J$.

Figure 9. (continued)

growing season (i.e., days ≈166 to 234). Indeed, the net effect of an increase in decomposition of surface litter is to decrease net mineralization by the same mechanism as that explaining Figure 7. On the contrary, the increase in J due to an increase in T_{soil} is weakened during the same period, for the net effect of an increase in decomposition of soil woody litter, soil herbaceous litter, active SOM, and slow SOM is to increase net mineralization. (Note the different scale of the vertical axes in Figures 9a and 9b.)

Figure 9c shows that an increase in air temperature (T_a) leads to a net decrease in J, which can be explained by a stronger increase in photosynthesis than in leaf respiration, except after the end of the growing season (i.e., after day 262). One sees that the sensitivity of J to T_a is dominated by two short periods. The high daily sensitivity to T_a between day 170 and day 173 and on day 241 is due to the fact that on these dates the actual leaf growth rate is equal to the potential leaf growth rate, which directly depends on T_a (equation (7)), whereas during the rest of the time it is limited by the amount of available photosynthate. The jump on day 241 is followed by a period of high sensitivity (i.e., 243 to 262) which coincides with the end of the growing season: on day 262, T_a becomes <-2°C so that photosynthesis stops. Note that there is no abrupt impact of T_a on J at the beginning of the growing season because photosynthesis remains very low during that period, due to the very small leaf biomass (equation (1)) which only gradually increases.

Figure 9d illustrates the fact that an increase in solar radiation results in higher photosynthesis rates and therefore lower J. For the same reason as in Figure 9c, J is very sensitive to a

time localized change in solar radiation occurring at the end of the growing season.

Finally, Figure 9e shows that an increase in soil moisture induces a decrease in J. This result is in agreement with measurements under controlled conditions by *Billings et al.* [1982]. Since in the chosen control conditions, an increase in soil moisture hinders decomposition, Figure 9e demonstrates that the net effect of a proportional decrease in decomposition of all soil organic matter pools (i.e., all decay rates multiplied by the same constant <1) is to decrease the annual net CO_2 flux, as shown also by the positive sensitivity to α in Table 4.

5. Limitation of the Adjoint Method

5.1. Comparison of the Adjoint Method With the Classical Method

How do the sensitivities computed by the adjoint model compare to those computed by the "classical" method? Let us consider the sensitivity of J with respect to cn. Let j_1 be the output of the direct model corresponding to control conditions ($cn_1 = cn$) and j_2 the output obtained for $cn_2 = cn + \delta cn$. The sensitivity computed by the classical method is $(j_2 - j_1)/\delta cn$. How does the output of the adjoint model, $\nabla_{cn} J$, compare to $(j_2 - j_1)/\delta cn$?

By definition of an adjoint operator (equation (19)) the adjoint variable corresponding to a perturbation δcn applied at time 0, cn_0^*, is exactly equal to the solution of the TLM, δJ, divided by the initial perturbation:

$$cn_0^* = \nabla_{cn} J = \frac{\delta J}{\delta cn} \tag{22}$$

This quantity compares well to the sensitivity given by the classical method, $(j_2 - j_1)/\delta cn$, when the output of the TLM, δJ is close to $(j_2 - j_1)$. Since by definition of the TLM, δJ is obtained by multiplying δcn by the tangent taken at each point of the control trajectory, δJ would be exactly equal to $(j_2 - j_1)$ if the direct model were linear (in that case, the control trajectory in the parameters and initial conditions space would be a straight line). In general, the direct model is nonlinear as in the present case, and δJ is a good approximation of $(j_2 - j_1)$ only for small enough changes in cn.

5.2. Presence of Thresholds

The present model contains not only nonlinear processes but also several relationships with thresholds or discontinuities, which are extreme cases of nonlinearity. For instance, the temperature dependence of decomposition is expressed by the function tfn which is nil for all temperatures below −7.5°C (equation (11)). There is thus a discontinuity in tfn at temperature $T = -7.5$°C. Therefore if the increment in temperature δT is large enough as to make $(T + \delta T) > -7.5$°C with $T < -7.5$°C, the run of the direct model corresponding to $(T + \delta T)$ will follow another trajectory than the control trajectory. If the evolution of a small perturbation is then computed using the TLM, which is determined by the trajectory of the control run, the result could be quite different than the evolution of a real, finite perturbation. In that case, the sensitivity computed with the adjoint would not represent correctly the sensitivity to a finite perturbation.

For $\delta T_s = 1$°C, Figure 10 shows that the cumulated change in CO_2 net flux computed by the TLM keeps drifting away from that computed by the direct method after the first threshold ($T_s = -7.5$°C) is encountered. Since an increase in T_s allows decomposition of surface litter to start earlier and finish later during the year, the direct run for $(T_s + \delta T_s)$ leads to a larger annual net flux, j_2, than the control value, j_1. Therefore $(j_2 - j_1)$ is much larger than the value δJ computed by the TLM, which only accounts for the impact of a larger T_s along the control trajectory without allowing the trajectory itself to change.

In the present model, six dependent variables are involved in processes with thresholds, i.e., T_{soil}, T_s, T_a, m, N_{min}, and B_2. Moreover, in the formulation of plant nutrient uptake the critical level of nutrient availability under which plant production is limited also defines a threshold (Figure 3, equation (14)). In the conditions chosen for the control run, only four out of the six dependent variables actually go through thresholds, namely, T_{soil}, T_s, T_a, and B_2, but increments in several NPP or decomposition parameters can induce trespassing of the critical level of nutrient availability.

In the present case, the TLM gives good approximations of $(j_2 - j_1)$ for changes in the initial rhizomes and stems biomass, $B_2(0)$, smaller or equal to $0.03B_2(0)$, and for increments of T_{soil}, T_s, and T_a of 0.5°C or less. We have thus to restrict our sensitivity analysis to perturbations of that order.

In conclusion, in the presence of thresholds or sharp nonlinearities, one has to define the maximum magnitude of the perturbations and the period of the run for which the gradients actually describe the response of the model to the perturbations, before using the gradients computed by the adjoint method in subsequent computation. To this end, we recommend to explicitly write the TLM code and check the similitude between the TLM results and the gradients computed by the direct method.

6. Discussion

6.1. Sensitivity of the Annual Net CO_2 Flux to Climate

The sensitivity curves of the annual net CO_2 flux to small perturbations of the climatic variables can help elucidate the short-term response of wet sedge tundra to climate change or interannual variability. Global circulation models (GCMs)

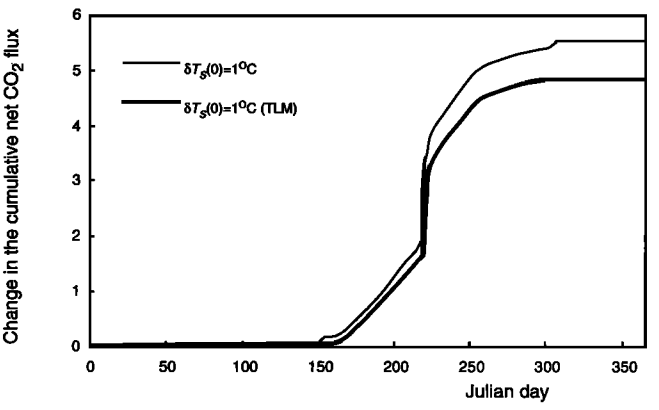

Figure 10. Cumulative variation in net CO_2 flux in response to $\delta T_s = 1$°C, computed by the LTM and by the direct method.

predict warming in high northern latitudes of 1° to 4°C in the summer and of 4° to 8°C in the winter in response to a growing season (i.e., days ≈166 to 243). Indeed, the net doubling of the atmospheric CO_2 concentration [*Mitchell et al.*, 1990]. Measurements of soil temperature profiles and surface weather records indicate that temperature in northern Alaska has increased by 2° to 4°C over the last few decades to century [*Lachenbruch et al.*, 1986; *Beltrami and Mareschal*, 1991; *Chapman and Walsh*, 1993], so that warming has already been taking place at rates ranging from 0.02° to possibly as much as 0.2°C yr^{-1}.

Because the adjoint results are only valid for small perturbations, they can only be used to study small departures from the control run. Therefore we analyze here the short-term response of the system to small changes in climatic conditions, such as those associated with the transient CO_2-induced warming or with interannual variability.

To estimate this response, one needs to distinguish between the five "climatic variables" concerned in the present study. Indeed, the soil temperature and moisture conditions, represented by T_s, T_{soil}, and m are interrelated and vary in response to changes in air temperature, solar radiation, and precipitation. We estimated the changes in T_s, T_{soil}, and m due to changes in air temperature and solar radiation with the help of a model of the soil thermal and hydrological regime in the presence of permafrost [*Waelbroeck*, 1993]. The net effect of a change in air temperature or solar radiation on the annual net CO_2 flux can then be assessed by adding up the effects of all the perturbed variables. Note that the fact that the sensitivity of the CO_2 flux to simultaneous changes in several parameters is simply the sum of the separate sensitivities is necessarily true for adjoint results because they only hold for perturbations such that the response of the model can be approximated by the local tangent to the model's trajectory. In contrast, sensitivities obtained by the classical method are not additive a priori.

Our results (Table 7) show that the response of the tundra to a 0.3°C increase in daily mean air temperature during a year is an 11.3% increase in annual CO_2 emission. This means that the short-term response of wet sedge tundra to CO_2-induced warming leads to a positive feedback to atmospheric CO_2 accumulation. The present results support findings by *Billings et al.* [1982] who observed a strong decrease in CO_2 net ecosystem uptake under elevated temperature in laboratory experiments. Moreover, a decrease in CO_2 net uptake has actually been recently observed in Barrow [*Oechel et al.*, 1994] and in other locations in northern Alaska [*Oechel et al.*, 1993]. It should be stressed that our results have to be understood as the change in annual net CO_2 flux due to a 0.3°C increase in air temperature applied during one year and cannot be interpreted as the ecosystem's response to climate change over 10 or 50 years. At these timescales, feedbacks due, among others, to changes in the nutrient cycling regime are likely to deeply modify the system's behavior.

We then explored how the natural climate interannual variability could modify the ecosystem's response to transient warming. As an example, we studied the effect of a 20 W m^{-2} decrease in solar radiation during the decomposition season. Such a decrease in solar radiation is equivalent to an increase in cloud cover of one to two tenths of sky area during the decomposition season. Table 7 shows that the effect of a 20 W m^{-2} decrease in solar radiation alone induces a 17.9% decrease in annual CO_2 emission. Note that a 20 W m^{-2} increase in solar radiation has a larger impact on J than a 20 W m^{-2} decrease because it has a larger impact on soil temperature and moisture, as predicted by the soil model

Table 7. Net Sensitivity to Climatic Change

Climatic Variable Changed		Variable Responding						Resulting δ (Annual Net Flux)		
		T_s		T_{soil}		m				
δclim	δJ, %	δT_s[a] (°C)	δJ, %	δT_{soil}[a] (°C)	δJ, %	δm[a] (% Dry Weight)	δJ, %	g C m^{-2} yr^{-1}	%	
T_a[b] + 0.3°C	−2.5	+0.32	+9	+0.23	+0.5	−7.6	+4.2	+1.92	+11.3	
S[c] + 20 W m^{-2}	−3	+0.43	+12.3	+0.29	+0.6	−23.9	+13.1	+3.89	+22.9	
S[c] − 20 W m^{-2}	+3	−0.32	−9.1	−0.23	−0.5	+20.7	−11.3	−3.04	−17.9	
T_a[b] + 0.3°C	−2.5									
S[c] − 20 W m^{-2}	+3	−0	−0	+0.03	+0.1	+14.1	−7.7	−1.20	−7.0	
		δT_s[d] (°C)		δT_{soil}[d] (°C)		δm[d] (% Dry Weight)				
T_a[b] + 0.3°C	−0.7	+0.39	+9.6	+0.26	−3.0	−4.7	+2.6	+1.19	+7.0	
		δT_s[e] (°C)		δT_{soil}[e] (°C)		δm[e] (% Dry Weight)				+13.1
T_a[b] + 0.3°C	−1.8									
S[f] − 20 W m^{-2}	+4.4	+0.04	+0.3	+0.07	+0.9	−7.5	+4.1	+1.03	+6.1	

[a]Induced change in average value during decomposition season.
[b]T_a is modified during the whole year.
[c]S is modified during the decomposition season (i.e., 156–311) only.
[d]Induced change in average value during 156–243 only.
[e]Induced change in average value during 244–311 only.
[f]S is modified during the second part of the decomposition season (i.e., 244–311) only.

used to assess changes in those input variables [*Waelbroeck*, 1993].

Interestingly, if a 20 W m^{-2} decrease in solar radiation during the decomposition season is superposed to the 0.3°C increase in air temperature due to the transient climate warming, the net result is a 7% decrease in CO_2 emission (Table 7). Therefore our results show that changes caused by the climate natural interannual variability (e.g., changes in cloudiness, precipitation) can severely alter and even mask the ecosystem response to transient climate warming.

Finally, since the effect of a change in a climatic variable depends very much on the time at which it takes place (section 4), it is interesting to estimate the impact of changes in cloudiness occurring during certain portions of the summer only. As explained in section 4.1, we can interpret the daily increment in the adjoint variable, $\xi^*_{n-1} - \xi^*_n$, as the impact on the annual net flux of a perturbation applied on day n. Consequently, the impact of perturbations applied during the first part of the period extending from day 156 to 243 is simply given by $\xi^*_{155} - \xi^*_{243}$. As an illustration, we estimate the impact of a 0.3°C increase in air temperature during the whole year, combined with a 20 W m^{-2} decrease in solar radiation during the second part of the decomposition season only (Table 7, bottom part). We obtain a 13.1% increase in CO_2 emission, which is radically different from the 7% decrease found when cloudiness increases during the whole summer. This shows that the actual short-term response of wet sedge tundra to climate changes not only depends on changes in cloudiness but also on the timing of these changes. Note that despite the increase in cloudiness predicted by GCMs in response to global warming, a decrease in cloudiness has been observed in recent years throughout the summer at Barrow (W. Oechel, personal communication, 1994). Our results therefore further support the increase in CO_2 emission observed in Barrow.

Although our results, strictly speaking, only concern wet sedge tundra, the fact that the sensitivity strongly depends on the period of the run during which the perturbation is applied is a general feature of systems encountering regime changes and hence of ecosystems. In this context, the adjoint method proves to be very convenient since it provides the full picture of the sensitivity to perturbations applied at any time of the run.

6.2. Conclusions

We developed a model of CO_2 exchange in tundra ecosystems and analyzed its sensitivity by the adjoint method. The adjoint method allowed us to obtain the sensitivities of the annual net CO_2 flux with respect to perturbations of the model's variables, climatic inputs, and main parameters on any day of the year, at minimal numerical cost. On one hand, our results show that the parameters which have the largest impact on CO_2 exchange in the tundra are decomposition parameters. This result is consistent with the fact that in nutrient-limited ecosystems, NPP is driven by nutrients availability, which is in turn driven by decomposition. On the other hand, we show that the short-term (1 year) response of wet sedge tundra to warming is an increase in CO_2 emission. When increases in cloudiness are taken into account, the response of the tundra can be either an increase in CO_2 emission or a decrease, depending on the period of the summer during which cloudiness increases. The technique we use in the present study to compute the sensitivity of the annual net CO_2 flux to small perturbations in several climatic inputs at various periods of the year is very general and can give estimates of the amplitude and sign of the short-term feedback to transient CO_2-induced climate change, provided that scenarios of predicted climate change are available.

Appendix A: Influence of the Substrate Chemical Composition and Soil Texture on Decomposition

The fraction of plant residue considered as woody litter is $0.15 + 0.018ln$; $ln \approx 40$, based on measurements by *Berendse and Jonasson* [1992]. In addition, the decomposition rate of woody litter depends on its lignin fraction, l_w:

$$K_1 = K_{\max 1} \exp(-3l_w)$$
$$K_3 = K_{\max 3} \exp(-3l_w) \tag{A1}$$

where $l_w \approx 0.25$ for tundra vegetation [*Miller et al.*, 1984].

Finally, the decay rate of active SOM located in mineral soil depends on soil texture:

$$K_5 = K_{\max 5}(1 - 0.75s) \tag{A2}$$

where s is the soil silt plus clay fraction; $s \approx 0.73$ at Barrow, based on measurements by *Brown et al.* [1980]. However, a fraction, f, of active SOM is located in the organic layer, for which the decay rate is $K_{\max 5}$. From current data on soil carbon content and bulk density, we can deduce $f \approx 0.26$.

In summary, the characteristic decay constants used in our control simulation at Barrow are the following:

$K_1 = 5.1 \times 10^{-3}$ day^{-1}	surface woody litter.
$K_2 = 40 \times 10^{-3}$ day^{-1}	surface herbaceous litter.
$K_3 = 6.3 \times 10^{-3}$ day^{-1}	soil woody litter.
$K_4 = 50 \times 10^{-3}$ day^{-1}	soil herbaceous litter.
$K_5 = 9 \times 10^{-3}$ day^{-1}	active SOM in mineral soil.
$K'_5 = 20 \times 10^{-3}$ day^{-1}	active SOM in organic soil.
$K_6 = 0.5 \times 10^{-3}$ day^{-1}	slow SOM.

Appendix B: Assessment of the Relative Content of the Active Layer SOM Pools

The budget equations of organic carbon in each active layer SOM pool can be written in a simplified form as

$$\frac{dC_i}{dt} = -k_i C_i + I_i \tag{B1}$$

where I_i represents the input flow to pool (i). If I_i and k_i are constant in time, the solution of (B1) with initial condition, $C_i(t = 0) = 0$, is

$$C_i(t) = \frac{I_i}{k_i}(1 - e^{(-k_i t)}) \tag{B2}$$

so that

$$C_i(t) \approx \frac{I_i}{k_i}$$
$$\frac{dC_i}{dt} \approx 0 \qquad \text{for } t \gg \frac{1}{k_i} \tag{B3}$$

Input flows I_i can be expressed as functions of the total litter input, I, assumed constant:

$$\begin{aligned} I_1 &= I(0.5)(0.15 + 0.018ln) \approx 0.435I \\ I_2 &= I(0.5)(0.85 - 0.018ln) \approx 0.065I \\ I_3 &= I_1 \\ I_4 &= I_2 \end{aligned} \tag{B4}$$

where half of the total litter is assumed to be surface litter and the other half, belowground litter. According to the flow diagram in Figure 1, I_5 and I_6 are linear combinations of the decomposition rates, k_iC_i; and according to (B3), k_iC_i can be approximated by I_i for $t \gg 1/k_i$. Thus

$$I_5 = (1 - l_w)0.55I_1 + (1 - l_w)0.45I_3 + 0.45(I_2 + I_4) + 0.45I_6$$

$$I_6 = l_w 0.7(I_1 + I_3) + (0.15 + 0.68s)I_5(1 - f) + 0.45fI_5 \tag{B5}$$

where $l_w = 0.25$, $s = 0.73$, and $f = 0.26$.

Substituting (B4) in (B5) gives the following solution:

$$I_5 \approx 0.620I; \qquad I_6 \approx 0.525I \tag{B6}$$

Consequently, for $t \to \infty$:

$$\begin{aligned} C_1 &\to \frac{0.435}{5.1 \times 10^{-3}} && \text{which represents 6.7\% of the total soil organic C} \\ C_2 &\to \frac{0.065}{0.04} && 0.1\% \\ C_3 &\to \frac{0.435}{6.3 \times 10^{-3}} && 5.4\% \\ C_4 &\to \frac{0.065}{0.05} && 0.1\% \\ C_5 &\to \frac{0.62f}{0.02} + \frac{0.62(1-f)}{9 \times 10^{-3}} && 4.7\% \\ C_6 &\to \frac{0.525}{0.0005} && 83.0\% \end{aligned} \tag{B7}$$

The total amount of soil organic carbon at Barrow is about 19,000 g C m^{-2} to a depth of 20 cm [*Chapin et al.*, 1980]. Therefore according to (B7), C_1 = 1272 g C m^{-2}, C_2 = 19 g C m^{-2}, C_3 = 1025 g C m^{-2}, C_4 = 19 g C m^{-2}, C_5 = 892 g C m^{-2}, and C_6 = 15,762 g C m^{-2}. Since the active layer is typically about 35-cm thick, 19,000 g C m^{-2} represent a lower limit of the total amount of active layer carbon.

Acknowledgments. We are grateful to Catherine Gautier for her initial push to start this study; to Walter Oechel, Steve Hastings, Mitch Jenkins, George Vourlitis, and Sarah Hobbie for field data and information; to Oliver Talagrand for discussions; and to Patrick Monfray and Philippe Ciais for the critical review of the manuscript. This work was supported by the CEA (C.W.), by NASA (grant NGT-30057, C.W.), and by the U.S. Department of Energy (grant DE-F602-90ER61065, J.-F.L.). This is contribution 165 of the LMCE.

References

Beltrami, H., and J.-C. Mareschal, Recent warming in eastern Canada inferred from geothermal measurements, *Geophys. Res. Lett.*, *18*, 605–608, 1991.

Berendse, F., and S. Jonasson, Nutrient use and nutrient cycling in northern ecosystems, in *Arctic Ecosystems in a Changing Climate*, edited by F. S. Chapin, R. L. Jefferies, J. R. Reynolds, G. R. Shaver, and J. Svoboda, pp. 337–356, Academic, San Diego, Calif., 1992.

Billings, W. D., J. O. Luken, D. A. Mortensen, and K. M. Peterson, Arctic tundra: A source or sink for atmospheric carbon dioxide in a changing environment?, *Oecologia*, *53*, 7–11, 1982.

Billings, W. D., K. M. Peterson, J. O. Luken, and D. A. Mortensen, Interaction of increasing atmospheric carbon dioxide and soil nitrogen on the carbon balance of the tundra microcosms, *Oecologia*, *65*, 26–29, 1984.

Bonan, G. B., A computer model of the solar radiation, soil moisture and soil thermal regimes in boreal forests, *Ecol. Modell.*, *45*, 275–306, 1989.

Brown, J., K. R. Everett, P. J. Webber Jr., S. F. Maclean, and D. F. Murray, The coastal tundra at Barrow, in An Arctic Ecosystem: The Coastal Tundra at Barrow, Alaska, edited by J. Brown, P. C. Miller, L. L. Tieszen, and F. L. Bunnell, *US/IBP Synth. Ser.*, *12*, 1–29, 1980.

Bunnell, F. L., and K. A. Scoullar, Abisko II, A computer simulation model of carbon flux in tundra ecosystems, in Structure and Function of Tundra Ecosystems, edited by T. Rosswall and O. W. Heal, *Ecol. Bull.*, *20*, 425–448, 1975.

Chapin, F. S., III, P. C. Miller, W. D. Billings, and P. I. Coyne, Carbon and nutrient budgets and their control in coastal tundra, in An Arctic Ecosystem: The Coastal Tundra at Barrow, Alaska, edited by J. Brown, P. C. Miller, L. L. Tieszen, and F. L. Bunnell, *US/IBP Synth. Ser.*, *12*, 458–482, 1980.

Chapman, W. L., and J. E. Walsh, Recent variations of sea ice and air temperature in high latitudes, *Bull. Am. Meteorol. Soc.*, *74*, 33–47, 1993.

Courtier, P., J. Derber, R. Errico, J.-F. Louis, and T. Vukićević, Important literature on the adjoint, variational methods and the Kalman filter in meteorology, *Tellus Ser. A*, *45*, 342–357, 1993.

Errico, R. M., and T. Vukićević, Sensitivity analysis using an adjoint of the PSU/NCAR mesoscale model, *Mon. Weather Rev.*, *120*, 1644–1660, 1992.

Flanagan, P. W., and A. K. Veum, Relationships between respiration, weight loss, temperature and moisture in organic residues on tundra, in *Soil Organisms and Decomposition in Tundra*, edited by A. J. Holding, O. W. Heal Jr., S. F. MacLean, and P. W. Flanagan, pp. 249–277, Tundra Biome Steering Committee, Stockholm, 1974.

Gates, W. L., J. F. B. Mitchell, G. J. Boer, U. Cubasch, and V. P. Meleshko, Climate modelling, climate prediction and model validation, in *Climate Change 1992, The Supplementary Report to the IPCC Scientific Assessment*, edited by J. T. Houghton, B. A. Callander, and S. K. Varney, pp. 97–134, Cambridge University Press, New York, 1992.

Grulke, N. E., G. H. Riechers, W. C. Oechel, U. Hjelm, and C. Jaeger, Carbon balance in tussock tundra under ambient and elevated atmospheric CO_2, *Oecologia*, *83*, 485–494, 1990.

Hall, M. C. G., D. G. Cacuci, and M. E. Schlesinger, Sensitivity analysis of a radiative-convective model by the adjoint method, *J. Atmos. Sci.*, *39*, 2038–2050, 1982.

Hoffman, R. N., J.-F. Louis, and T. Nehrkorn, A method for implementing adjoint calculations in the discrete case, *Tech. Memo. 184*, 19 pp., Eur. Cent. for Medium Range Weather Forecasts, Reading, England, 1992.

Jenkinson, D. S., D. E. Adams, and A. Wild, Model estimates of CO_2 emissions from soil in response to global warming, *Nature*, *351*, 304–306, 1991.

Lachenbruch, A. H., and B. V. Mareschal, Changing climate: Geothermal evidence from permafrost in the Alaskan arctic, *Science*, *234*, 689–696, 1986.

Le Dimet, F.-X., and O. Talagrand, Variational algorithms for analysis and assimilation of meteorological observations: Theoretical aspects, *Tellus Ser. A*, *38*, 97–110, 1986.

Limbach, W. E., W. C. Oechel, and W. Lowell, Photosynthetic and respiratory responses to temperature and light of three Alaskan tundra growth forms, *Holarctic Ecol.*, *5*, 150–157, 1982.

Louis, J.-F., and M. Živković, Optimizing a local weather forecast model, final report, contract ISI-9100720, 55 pp., Natl. Sci. Found., Washington, D. C., 1994. (Available from Atmospheric and Environmental Research, Inc., Cambridge, Mass.)

Miller, P. C., et al., Plant-soil processes in Eriophorum vagitum tussock tundra in Alaska: A systems modelling approach, *Ecol. Monogr.*, *54*, 361–405, 1984.

Mitchell, J. F. B., S. Manabe, V. Meleshko, and T. Tokioka, Equilibrium climate change—and its implications for the future, in *Climate Change, the IPCC Scientific Assessment*, edited by J. T. Houghton, G. J. Jenkins, and J. J. Ephraums, pp. 131–172, Cambridge University Press, New York, 1990.

Nadelhoffer, K. J., A. E. Giblin, G. R. Shaver, and J. A. Laundre, Effects of temperature and substrate quality on element mineralization in six arctic soils, *Ecology*, *72*, 242–253, 1991.

Oechel, W. C., and W. D. Billings, Effects of global change on the carbon balance of Arctic plants and ecosystems, in *Arctic Ecosystems in a Changing Climate*, edited by F. S. Chapin, R. L. Jefferies, J. R. Reynolds, G. R. Shaver, and J. Svoboda, pp. 139–168, Academic, San Diego, Calif., 1992.

Oechel, W. C., S. J. Hastings, G. L. Vourlitis, M. Jenkins, G. H. Riechers, and N. E. Grulke, Recent change in Arctic tundra ecosystems from a net carbon dioxide sink to a source, *Nature*, *361*, 520–523, 1993.

Oechel, W. C., G. L. Vourlitis, S. J. Hastings, and S. A. Bochkarev, Change in Arctic CO_2 flux over two decades: Effects of climate change at Barrow, Alaska, *Ecol. Appl.*, in press, 1994.

Parton, W. J., D. S. Schimel, C. V. Cole, and D. S. Ojima, Analysis of factors controlling soil organic matter levels in great plains grasslands, *Soil Sci. Soc. Am. J.*, *51*, 1173–1179, 1987.

Rastetter, E. B., M. G. Ryan, G. R. Shaver, J. M. Mellillo, K. J. Nadelhoffer, J. E. Hobbie, and J. D. Aber, A general biogeochemical model describing the responses of the C and N cycles in terrestrial ecosystems to changes in CO_2, climate and N deposition, *Tree Physiol.*, *9*, 101–126, 1991.

Running, S. W., and J. C. Coughlan, A general model of forest ecosystem processes for regional applications, I, Hydrologic balance, canopy gas exchange and primary production processes, *Ecol. Modell.*, *42*, 125–154, 1988.

Schlesinger, M. E., and J. F. B. Mitchell, Climate model simulations of the equilibrium climatic response to increased carbon dioxide, *Rev. Geophys.*, *25*, 760–789, 1987.

Shaver, G. R., and F. S. Chapin, Production: Biomass relationships and element cycling in contrasting Arctic vegetation types, *Ecol. Monogr.*, *61*, 1–31, 1991.

Shaver, G. R., and J. Kummerow, Phenology, resource allocation, and growth of Arctic vascular plants, in *Arctic Ecosystems in a Changing Climate*, edited by F. S. Chapin, R. L. Jefferies, J. R. Reynolds, G. R. Shaver, and J. Svoboda, pp. 193–211, Academic, San Diego, Calif., 1992.

Talagrand, O., and P. Courtier, Variational assimilation of meteorological observations with the adjoint vorticity equation, I, Theory, *Q. J. R. Meteorol. Soc.*, *113*, 1311–1328, 1987.

Thépaut, J.-N., and P. Moll, Variational inversion of simulated TOVS radiances using the adjoint technique, *Q. J. R. Meteorol. Soc.*, *116*, 1425–1448, 1990.

Tieszen, L. L., Photosynthesis in vascular plants, in *Vegetation and Production Ecology of an Alaskan Arctic Tundra*, edited by L. L. Tieszen, pp. 241–268, Springer-Verlag, New York, 1978.

Tissue, D. T., and W. C. Oechel, Response of eriophorum vaginatum to elevated CO_2 and temperature in the Alaskan tussock tundra, *Ecology*, *68*, 401–410, 1987.

Waelbroeck, C., Climate-soil processes in the presence of permafrost: A systems modelling approach, *Ecol. Modell.*, *69*, 185–225, 1993.

J.-F. Louis, Atmospheric and Environmental Research, Inc., 840 Memorial Drive, Cambridge, MA 02139.

C. Waelbroeck, Laboratoire de Modelisation du Climat et de l'Environnement, CE Saclay, Orme des Merisiers, 91191 Gif-sur-Yvette Cédex, France.

(Received July 12, 1994; revised October 25, 1994; accepted October 28, 1994.)